Impacts of Reliability-Oriented Phase Shedding in Modular Dab Ev Charging

Impacts of Reliability-Oriented Phase Shedding in Modular DAB EV Charging

Jiayi Geng
Dept. of Electrical, Electronic, and Information Engineering
University of Bologna
Bologna, Italy
jiayi.geng3@unibo.it

Riccardo Mandrioli
Dept. of Electrical, Electronic, and Information Engineering
University of Bologna
Bologna, Italy
r.mandrioli@unibo.it

Ariya Sangwongwanich
Dept. of Energy
Aalborg University
Aalborg, Denmark
ars@energy.aau.dk

Mattia Ricco
Dept. of Electrical, Electronic, and Information Engineering
University of Bologna
Bologna, Italy
mattia.ricco@unibo.it

***Abstract*—The efficiency and reliability performance of various power sharing strategies for a modular electrical vehicle charging system are evaluated. The dual-active-bridge converters are employed due to their adaptability and robust performance. Considering reliability and overall efficiency, power-sharing strategies based on module-shedding effectively improve system efficiency under light-load conditions, while rotating module-shedding can increase reliability by evenly distributing thermal stress among the modules. However, the performance of rotating module-shedding is dependent on the rotating frequency. To analyze the advantages and limitations of various power-sharing strategies, this paper compares their performance from the perspective of reliability and efficiency, which can provide a guideline for selecting the suitable power-sharing strategy based on specific system performance requirements.**

***Index Terms*—Dual Active Bridge, Efficiency, EV charging, Power losses, Reliability**

I. Introduction

To meet the growing demand for green mobility, the increasing number of electric vehicles (EVs) necessitates faster charging rates, which require high-performance DC/DC converters and robust system power management strategies capable of high current and power levels. For reliability and redundancy, fast EV supply equipment (EVSE) typically employs modular configurations [1]. The dual-active-bridge (DAB) converter has gained significant attention for EV fast-charging applications due to its voltage step-up/down, galvanic isolation, and high-power processing capabilities [2]. Furthermore, it supports a simple modulation technique, single-phase-shift (SPS), which can achieve high efficiency, especially in high-power application by enabling soft switching through the phase shift adjustment between the full-bridge [3]. However, power electronic switches in EV fast-charging systems are inevitably subjected to high levels of voltage and current stress, which poses a challenge to system reliability [4]–[6].

This study was carried out within the MOST–Sustainable Mobility Center and received funding from the European Union Next-GenerationEU (piano Nazionale di ripresa e resilienza (PNRR) missione 4, componente 2, investimento 1.4–D.D. 1033 17/06/2022, CN00000023). This manuscript reflects only the authors' views and opinions; neither the European Union nor the European Commission can be considered responsible for them.

Jiayi Geng acknowledges the financial support from the China Scholarship Council (Grant No.202308130048).

In virtue of the EV charging application-specific requirements, EVSEs experience stochastic and time-varying load according to EV model, state-of-charge, and ambient temperature, which can cause power converter junction temperature fluctuation and suboptimal utilization [7]. Therefore, to optimize system reliability and efficiency, appropriate power-sharing strategies (PSSs) capable of allocating charging load among EVSE modules are necessary. The simplest PSS can be realized by evenly sharing the charging power across all the modules simultaneously. However, this PSS tends to result in low efficiency under light-load conditions [8]. A common solution is to dynamically activate the optimal number of modules using module-shedding approach based on the actual load conditions. The number of active modules can be determined in real-time considering the module's rated power and efficiency [9]–[11]. In the literature, conventional module shedding tends to prioritize the first modules, while high-order modules are utilized only during brief power peaks (e.g., low state-of-charge operations). In the long term, this results in an imbalanced distribution of loading and utilization among the modules, leading to uneven thermal stress, thus reducing system reliability [12], [13]. To mitigate this issue, rotating phase shedding has been proposed as an improved thermal management strategy [14]. However, the rotating frequency is a critical parameter that has not been thoroughly analyzed yet. In fact, inappropriate values can lead to junction temperature periodic fluctuations, which negatively affect both reliability and the overall efficiency [8].

This paper investigates the impact of nine different PSSs on the EV charging system, including even power sharing, maximum power-oriented module-shedding, and efficiency-oriented module-shedding as well as multiple module rotation strategies and frequencies. The objective is to evaluate the reliability and efficiency performance of the various PSSs, providing guidance for selecting an optimal power-sharing strategy for achieving a trade-off between reliability and efficiency.

The rest of the paper is organized as follows. Section II presents the working requirements and design parameters of the EV charging system. A one-year mission profile used for performance evaluation and a detailed description of the nine PSSs are indicated in Section III. The efficiency and reliability evaluation procedures and results analysis are provided in Section IV. Finally, Section V summarizes the study and future research directions.

II. EV Charging System and Thermal Design

A. EV Charging System Description

To handle the high power demand of the EV charging system, the 10-module DAB structure visible in Fig. 1 has been selected. Each DAB module is rated 25 kW, and it is operated employing the SPS modulation technique [3]. The total output power P_o is therefore set to 250 kW. Each module delivers a maximum output voltage V_{o} of 500 V, and for applications requiring higher battery charging voltages (i.e., EV with 800 V batteries), pairs of module outputs are reconfigured into a series connection, forming a configuration with five couples of modules. Moreover, for optimizing system reliability and fault tolerance, two MOSFETs are connected in parallel per leg within each module, employing Wolfspeed SiC MOSFETs C2M0040120D (1200 V, 60 A) and C3M0025065K (650 V, 97 A) on the primary and the secondary side, respectively. The operational parameters of the converter are shown in Table I.

B. Thermal Design

A comprehensive reliability and efficiency assessment of the converter system requires consideration of the cooling system design, as this defines the electrical and thermal behavior for the system. The conduction and commutation losses analysis of the switching devices is a critical procedure in the design of the thermal system. The applied loss evaluation method relies on the component thermal description in the form of look-up tables (LUTs) generated from datasheet information. This procedure allows taking into account the actual voltage, power, and junction temperature along the mission profile [15]. Simulations were performed in PLECS (Plexim GmbH) environment across various operating conditions, including power levels from 0 kW to 25 kW, output voltages ranging from 50 V to 600 V, and junction temperatures from -10 °C to 180 °C. These simulations generated 3D LUTs to characterize losses as functions of power, output voltage.

In this design, the Cauer RC thermal network is employed. Each half-bridge (i.e., four devices in total) is equipped with an individual heatsink, so the thermal chain of each half-bridge includes four parallel junction-to-case (Z_{jc}) and case-to-heatsink (Z_{ch}), a series heatsink-to-ambient thermal impedance (Z_{ha}). Therefore, the device steady state junction temperature is found as:

$$T_{\mathrm{j}} = P_{\mathrm{loss}} \left(R_{\mathrm{jc}} + R_{\mathrm{ch}}\right) + 4P_{\mathrm{loss}} R_{\mathrm{ha}} + T_{\mathrm{a}} \ , \qquad (1)$$

where T_{j} and P_{loss} are the junction temperature and power loss of a single switching device, respectively. R_{jc}, R_{ch} and R_{ha} represent the thermal resistances.

The Z_{jc} are derived from MOSFETS' datasheets, as shown in Table II. The thermal interface material resistance R_{ch} is evaluated, as it depends on the specific device dimensions and materials, while the heatsink-to-ambient thermal resistances is calculated according to (1) to ensure safe junction temperatures under full load conditions, where the value of P_{loss} can be derived from the LUTs. This maintains device operation within the allowable temperature range of 150 °C under an ambient temperature of 40 °C. The corresponding values are provided in Table III.

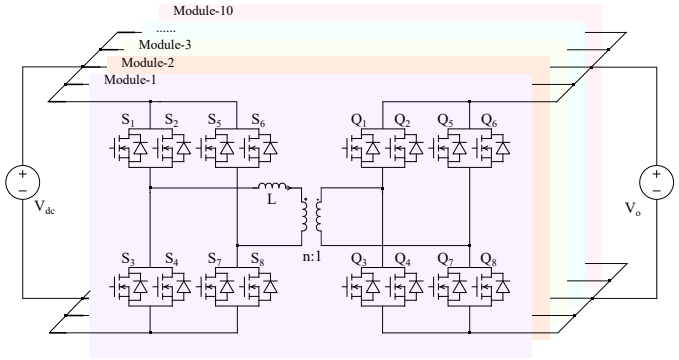

Fig. 1: Architecture of the 10-module DAB.

TABLE I: Main System Parameters.

Description	Symbol	Value	Units
Input Voltage	V_{dc}	800	V
Maximum Output Voltage	V_{max}	500	V
Total Power	P_{max}	250	kW
DAB Maximum Power	P_{max1}	25.0	kW
DAB Peak Efficiency Point	P_{η}	8.14	kW
Switching Frequency	f	50	kHz
Inductance Value	L	57.2	μH
Transformer Ratio	n : 1	2 : 1	-
Total Number of DAB Module	N	10	-

TABLE II: Cauer thermal model for the selected MOSFETs.

Side	Z_{jc}	Cauer Thermal Model				Unit
Primary†	R_{jc}	25.8	85.7	84.2	182	mK/W
	C_{jc}	6.30	16.5	112	359	mJ/K
Secondary‡	R_{jc}	67.7	187	86.2	116	mK/W
	C_{jc}	1.30	6.30	21.4	51.7	mJ/K

† C2M0040120D; ‡ C3M0025065K

TABLE III: Cauer thermal parameters from case to ambient.

Parameter	Symbol	Value	Unit
Case-to-heatsink	R_{ch}	4.70	mK/W
Heatsink-to-ambient	R_{ha}	913	mK/W
	C_{ha}	5.35	J/K

III. Mission Profile and Power-Sharing Strategies

A. EV Charging Mission Profile Determination

The one-year mission profile visible in Fig. 2 has been generated in a randomized way assuming a population of 16 EVs and considering arrival and departure times from the city center scenario discussed in [16] and the initial state of charge from [17]. Every day accounts on average of about 12 charging events. The ambient temperature has been generated considering daily mean average, mean maximum, and mean minimum temperatures from historical data ranging from the period 1991-2020 in the city of Bologna (the same city examined in [16], [17]). Mission profile data is generated with a time resolution of 1 minute.

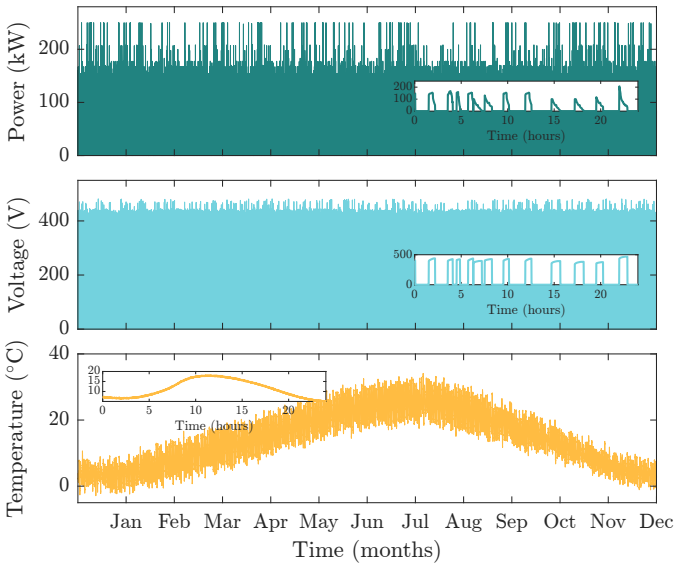

Fig. 2: One-year mission profile output power (top), output voltage (middle), and ambient temperature in Bologna (bottom). Zoom frames show one-day time span.

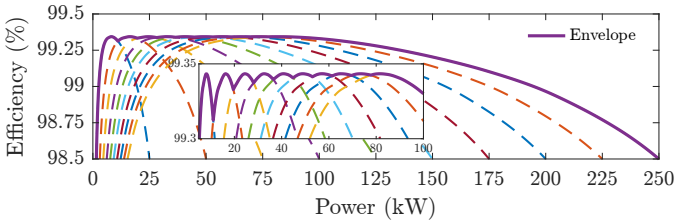

Fig. 3: Efficiency curve of modular DAB converter with efficiency-oriented module-shedding at 400 V and 100 °C.

B. Modular DAB Power-Sharing Strategies

To enable suitable result comparison regarding reliability and efficiency, nine PSSs have been developed in this subsection, including even sharing, power-oriented module-shedding, and efficiency-oriented module-shedding strategies. To analyze the load switching points for efficiency-oriented module-shedding in the modular DAB converter studied in this paper, the total loss of one DAB module assuming to operate at a junction temperature of 100 °C, an output voltage of 400 V, and different power levels are calculated based on the LUTs. According to the losses analysis, a typical efficiency curve for the modular configuration with efficiency-oriented module-shedding is presented in Fig. 3, where N is the active number of DAB modules. The load switching points can be identified in Fig. 3 and used as the reference points for module-shedding, ensuring that the system operates at optimal efficiency conditions (shown by the envelope line in Fig. 3). Every PSS allocated the mission profile visible in Fig. 2 among the 10 DAB modules differently. Fig. 4 illustrates the power distribution among 10 DAB modules in case of different PSSs. t_{on} represents the percentage of active time for each module over one year. The average power during active periods has been indicated with dashed lines in Fig. 4. PSSs detailed explanation is as follows:

- **PSS 1:** The load is evenly shared among the 10 DAB modules regardless of the power level. As per Fig. 4, all the modules share the same average powers and active times;
- **PSS 2:** The load is split into 25 kW chunks and sequentially allocated among the modules from DAB-1 to DAB-10 (i.e., maximum power-oriented module-shedding). As displayed in Fig. 4, power is allocated mostly in low-order modules (i.e., from DAB-1 to DAB-4). High-order modules present a particularly low level of utilization (i.e., < 1 %), which results in a sequential decrease in their active time;

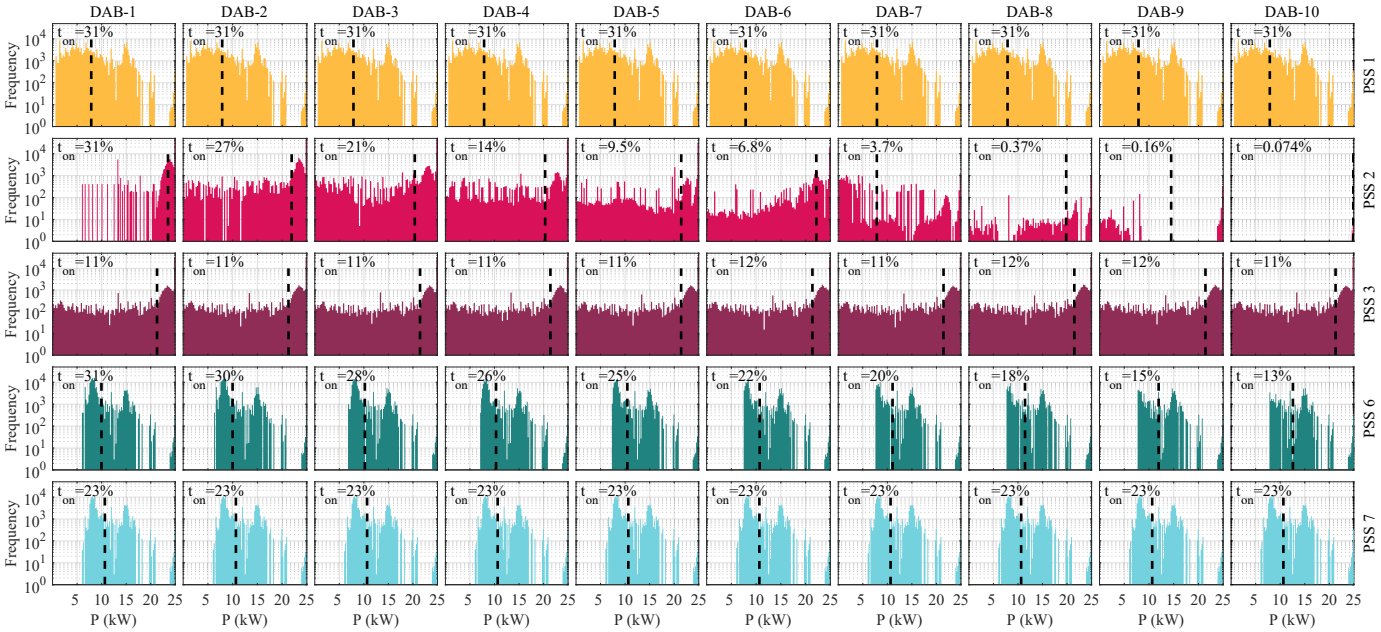

Fig. 4: Histogram of the yearly power P allocation among the 10 DAB modules (left to right) in case of PSS 1, PSS 2, PSS 3, PSS 6, and PSS 7 (from top to bottom). Dashed lines indicate average power (when active) and t_{on} the active time in percentage.

- **PSS 3:** Power division equivalent to **PSS 2**. DAB modules are sequentially rotated at every charging event. Thanks to the rotation, power allocation and active time shown in Fig. 4 assume an almost perfect balance among the modules;
- **PSS 4:** Same as **PSS 3** but the rotation is randomized at every charging event;
- **PSS 5:** Power division equivalent to **PSS 2**. DAB modules are randomly rotated every minute—high-frequency rotation;
- **PSS 6:** The load is split and sequentially allocated among the DAB modules following an efficiency-oriented module-shedding as per Fig. 3 [9], [18]. Despite no rotation, the reference power for module-shedding is lower than 25 kW specified in **PSS 2**, the utilization frequency of high-order modules increases. Therefore, the active times are improved and power discrepancies visible in Fig. 4 among the modules are less severe if compared to **PSS 2**;
- **PSS 7:** Power division equivalent to **PSS 6**. DAB modules are sequentially rotated at every charging event (likewise **PSS 3**). As displayed in Fig. 4, also in this case the rotation allows for a balance of the power allocation among the modules. If compared to **PSS 3**, active times are higher but the average power is lower;
- **PSS 8:** Same as **PSS 7** but the rotation is randomized at every charging event (likewise **PSS 4**);
- **PSS 9:** Power division equivalent to **PSS 6**. DAB modules are randomly rotated every minute (likewise **PSS 5**).

PSSs not displayed in Fig. 4 present histograms similar to the already displayed one. Specifically, **PSS 4** and **PSS 5** presents values similar to **PSS 3** while **PSS 8** and **PSS 9** replicate **PSS 7**.

The number of active DABs N_a at a given load P_o is:

$$N_\mathrm{a} = \begin{cases} N & \textbf{PSS 1} \\ \left\lceil N \frac{P_\mathrm{o}}{P_\mathrm{max}} \right\rceil & \textbf{PSS 2-5} \\ \left\lceil \sqrt{\frac{1}{4} + \frac{P_\mathrm{o}^2}{P_\eta^2}} - \frac{1}{2} \right\rceil & \textbf{PSS 6-9} \end{cases}, \tag{2}$$

having P_η the peak efficiency point of a single DAB and $N_\mathrm{a} \leq N$ [9]. A visual representation of the different values of N_a resulting from (2) is available in Fig. 5. As the power range and modulation strategy change, the number of activated DAB modules also varies. For **PSS 1**, all 10 modules operate simultaneously under any power requirement, as shown in Fig. 3. Comparing the two module-shedding strategies, it stands clear that efficiency-oriented module-shedding (**PPS 6** - **PSS 9**) inherently shares more equally the power among modules because it engages all modules already from about 30 % of P_max. On the other hand, maximum power-oriented module-shedding (**PPS 2** - **PSS 5**) must rely on DAB rotation for distributing the stress among the modules.

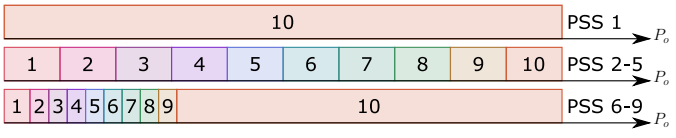

Fig. 5: Comparison between even sharing (top), maximum power-oriented module-shedding (middle), and efficiency-oriented module-shedding (bottom) PSSs. Numbers indicate how many DAB modules are active for a given value of output power P_o.

IV. Results and Discussion

A. Lifetime Evaluation Methodology

As shown in Fig. 4, under the same mission profile, the uneven power distribution across different PSSs leads to unequal aging performance of modules and affects overall system efficiency.

To further analyze the impact, the 3D LUTs have been generated to characterize the power losses of each switching device within a DAB module. Based on the mission profile of individual DAB modules under different PSSs, as shown in Fig. 4, along with the developed thermal model and LUTs, the power loss and junction temperature profiles of the switching devices can be derived. By analyzing the power loss results, the average efficiency of the system over the active periods in one year has been calculated, as listed in Table IV.

To examine the irregular temperature fluctuations caused by the dynamic mission profile, a rainflow-counting algorithm is used to transform these fluctuations into regular thermal loading cycles to be fed into the lifetime model to estimate the number of failure cycles for the switching devices [15]. The Bayerer's lifetime model from [19] is employed. It establishes the relationship between the number of cycles to failure (N_f) and the junction thermal parameters as:

$$N_\mathrm{f} = A\, \Delta T_\mathrm{j}^{-\beta_1}\, e^{\frac{\beta_2}{T_\mathrm{jm}+273}}\, t_\mathrm{on}^{\beta_3}\, I^{\beta_4}\, V^{\beta_5}\, D^{\beta_6}\,, \tag{3}$$

where I, V, and D are current per bond wire, blocking voltage, and bond wire diameter. T_jm is the minimum junction temperature in °C while ΔT_j is the junction temperature swing. A and $\beta_1 - \beta_6$ are empirical parameter and model parameters from [19]. Typically, Miner's rule is applied to calculate life consumption by accumulating damage contributions from each thermal cycle to predict device lifetime.

As shown in Fig. 1, the failure of any switching device results in a reduction of the system power handling capability. Therefore, to assess system reliability while maintaining the original rated power, as illustrated in Fig. 6 a series reliability block diagram (RBD) is employed at the converter/module level to account for the independence of the component reliability. Similarly, system-level reliability is determined by aggregating the reliability of individual converters arranged in a series RBD. In practical reliability analysis, results derived from lifetime model often tend toward idealized values due to various uncertainties. To address this, the Monto Carlo analysis is utilized, using statistical failure probabilities to represent the reliability of devices and systems. This approach incorporates parameter variations and models lifetime consumption, with the results fitted using Weibull distribution [20]. The reliability results at the module and system level are presented in Table IV.

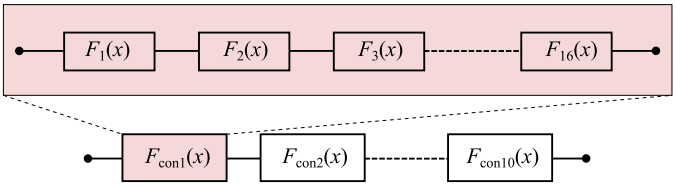

Fig. 6: Series reliability block diagram of the 10-DAB system. Each DAB module contains 16 switching devices.

TABLE IV: DAB- AND SYSTEM-LEVEL B1 LIFETIME† TOGETHER WITH SYSTEM-LEVEL EFFICIENCY‡ ASSESSMENT.

Strategies	DAB-1	DAB-2	DAB-3	DAB-4	DAB-5	DAB-6	DAB-7	DAB-8	DAB-9	DAB-10	B1 Lifetime	Efficiency
PSS 1	34.4	34.4	34.4	34.4	34.4	34.4	34.4	34.4	34.4	34.4	11.6	98.80 %
PSS 2	8.00	8.40	14.0	17.6	27.2	4.00	85.2	152	982	941	3.20	98.32 %
PSS 3	12.8	13.6	13.6	14.0	13.2	13.2	13.6	13.6	13.2	13.6	3.60	98.32 %
PSS 4	13.2	13.6	12.4	13.2	13.6	14.0	12.8	16.8	13.6	13.6	4.00	98.26 %
PSS 5	< 1	< 1	< 1	< 1	< 1	< 1	< 1	< 1	< 1	< 1	< 1	98.62 %
PSS 6	23.2	25.6	32.4	37.6	44.4	65.6	99.2	187	190	196	13.2	98.97 %
PSS 7	48.4	48.0	49.6	50.0	48.4	47.6	48.8	47.2	48.0	48.0	15.6	98.97 %
PSS 8	47.6	50.0	47.2	47.6	48.8	49.6	47.6	48.8	48.4	48.4	15.6	98.97 %
PSS 9	47.6	47.2	48.8	46.4	46.8	46.8	48.4	46.4	46.0	45.6	15.2	98.97 %

† B1 lifetime is expressed in years.
‡ Global efficiency not accounting for transformers' losses.

B. Efficiency and Lifetime Discussion

With reference to the mission profile introduced in Subsection III-A, the 9 PSSs have been numerically evaluated for all 10 DAB modules. Rresults are available in Table IV.

PSS 1 shows better B1 lifetime and efficiency than **PSS 2** - **PSS 5**. The B1 lifetime decrease of about 8 years is due to DAB modules consistently operating at full load, making their performance the determining factor for the system. In contrast, **PSS 6** - **PSS 9** optimize the number of active modules based on load requirements, resulting in a 0.17 % efficiency improvement and B1 lifetime increment up to 4 years if compared to **PSS 1**. This is due to the minimization of full-load operations.

System efficiency under the two module-shedding strategies is comparable. However, in **PSS 2** and **PSS 6**, the uneven power allocation leads to significant differences in module lifetime. In **PSS 2**, the lifetime difference between the most and the least reliable modules reaches 978 years, while the difference in **PSS 6** is about 172.8 years. The module with the lowest reliability limits the system's reliability performance, resulting in a shorter system lifetime. In contrast, rotating power-sharing strategies (**PSS 3** and **PSS 7**) equalize the reliability performance of the 10 DAB modules.

The three rotating PSSs exhibit distinct behaviors. Despite having the same rotation frequency, random rotation **PSS 4** reduces system efficiency by 0.06 % but improves reliability by about 0.4 years if compared with **PSS 3**. However, when the rotation frequency increases to 1 minute (**PSS 5**), the system efficiency improves by 0.3 % while more frequent thermal oscillations lead to a negative impact on the B1 lifetime, reducing it below 1 year. For efficiency-oriented module-shedding, **PSS 7** - **PSS 9** show similar efficiency performance. Under the same rotating frequency, random rotation (**PSS 8**) has minimal impact on reliability. Comparing **PSS 8** and **PSS 9**, lifetime decreases with higher rotation frequencies, though not as rapidly as in **PSS 5**.

Overall, efficiency-oriented module-shedding proves beneficial for improving both system reliability and efficiency. For efficiency-dominated scenarios, the traditional efficiency-oriented module-shedding method (**PSS 6**) is sufficient. When reliability is a priority, module-shedding with rotation (**PSS 7**) is recommended. Rotating modules once every EV charging event proves to be sufficient.

V. CONCLUSION

This paper introduces the reliability and efficiency performance of a modular DAB converter operating under nine different power-sharing strategies with the same mission profile. Efficiency-oriented module-shedding proves to be an effective method for enhancing both system efficiency and reliability. While module-shedding with rotation does not improve efficiency, it is valuable in equalizing reliability across modules, thereby contributing positively to the overall system reliability. Overall, power-sharing strategies with different rotation logic have minimal impact on system efficiency and reliability; however, the rotation frequency plays a critical role. A sufficiently low rotation frequency can lead to uneven thermal performance, reducing the reliability benefits, while an excessively high frequency can increase thermal oscillations, which degrade system reliability. Therefore, determining the optimal rotation frequency for efficiency-oriented module-shedding is crucial to balance thermal management, efficiency, and reliability. The optimization of this variable is currently being studied and will be presented in future research.

REFERENCES

[1] K. Drobnic, G. Grandi, M. Hammami, R. Mandrioli, M. Ricco, A. Viatkin, and M. Vujacic, "An output ripple-free fast charger for electric vehicles based on grid-tied modular three-phase interleaved converters," *IEEE Transactions on Industry Applications*, vol. 55, no. 6, pp. 6102–6114, 2019.

[2] S. Cuoghi, L. K. Pittala, R. Mandrioli, V. Cirimele, M. Ricco, and G. Grandi, "Model-based adaptive control of modular dab converter for ev chargers," *IET Power Electronics*, vol. n/a, no. n/a.

[3] R. De Doncker, D. Divan, and M. Kheraluwala, "A three-phase soft-switched high-power-density dc/dc converter for high-power applications," *IEEE Transactions on Industry Applications*, vol. 27, no. 1, pp. 63–73, 1991.

[4] J. He, A. Sangwongwanich, Y. Yang, and F. Iannuzzo, "Lifetime evaluation of three-level inverters for 1500-v photovoltaic systems," *IEEE Journal of Emerging and Selected Topics in Power Electronics*, vol. 9, no. 4, pp. 4285–4298, 2021.

[5] J. Karunarathna, U. Madawala, C. Baguley, F. Blaabjerg, and M. Sandelic, "Reliability analysis of fast electric vehicle charging systems," in *2021 IEEE 12th Energy Conversion Congress & Exposition - Asia (ECCE-Asia)*, 2021, pp. 1607–1612.

[6] P. D. Reigosa, H. Wang, Y. Yang, and F. Blaabjerg, "Prediction of bond wire fatigue of igbts in a pv inverter under a long-term operation," *IEEE Transactions on Power Electronics*, vol. 31, no. 10, pp. 7171–7182, 2016.

[7] H. Polat, F. Hosseinabadi, S. Chakraborty, T. Geury, M. El Baghdadi, and O. Hegazy, "Assessing the impact of ev charging and discharging profiles on t-type active front end charger lifetime," in *IECON 2023- 49th Annual Conference of the IEEE Industrial Electronics Society*, 2023, pp. 1–7.

[8] M. A. Alharbi, A. M. Alcaide, M. Dahidah, M.-R. P., S. Ethni, V. Pickert, and J. I. Leon, "Rotating phase shedding for interleaved dc–dc converter-based evs fast dc chargers," *IEEE Transactions on Power Electronics*, vol. 38, no. 2, pp. 1901–1909, 2023.

[9] J. W. Kolar, F. Krismer, Y. Lobsiger, J. Muhlethaler, T. Nussbaumer, and J. Minibock, "Extreme efficiency power electronics," in *2012 7th International Conference on Integrated Power Electronics Systems (CIPS)*, 2012, pp. 1–22.

[10] G. Son, Z. Huang, and Q. Li, "Light load efficiency improvement for two-channel paralleled soft-switching three-phase inverter using phase shedding control," *IEEE Transactions on Power Electronics*, vol. 37, no. 9, pp. 10 200–10 212, 2022.

[11] X. Zhou, M. Donati, L. Amoroso, and F. Lee, "Improved light-load efficiency for synchronous rectifier voltage regulator module," *IEEE Transactions on Power Electronics*, vol. 15, no. 5, pp. 826–834, 2000.

[12] Z. Xiao, Z. Yao, F. Deng, L. Zhang, and Y. Tang, "Seamless rotational phase shedding for multiphase dc–dc converters," *IEEE Transactions on Power Electronics*, vol. 39, no. 5, pp. 4996–5001, 2024.

[13] G. Yedukondalu and S. Samanta, "Effective phase utilization and efficiency improvement of high power interleaved dc–dc converter using modified rotating phase shedding control," *Computers and Electrical Engineering*, vol. 110, p. 108837, 2023.

[14] Y. Ahn, I. Jeon, and J. Roh, "A multiphase buck converter with a rotating phase-shedding scheme for efficient light-load control," *IEEE Journal of Solid-State Circuits*, vol. 49, no. 11, pp. 2673–2683, 2014.

[15] A. Sangwongwanich, Y. Yang, D. Sera, and F. Blaabjerg, "Lifetime evaluation of grid-connected pv inverters considering panel degradation rates and installation sites," *IEEE Transactions on Power Electronics*, vol. 33, no. 2, pp. 1225–1236, 2018.

[16] F. Lo Franco, M. Ricco, V. Cirimele, V. Apicella, B. Carambia, and G. Grandi, "Electric vehicle charging hub power forecasting: A statistical and machine learning based approach," *Energies*, vol. 16, no. 4, 2023.

[17] F. Lo Franco, V. Cirimele, M. Ricco, V. Monteiro, J. L. Afonso, and G. Grandi, "Smart charging for electric car-sharing fleets based on charging duration forecasting and planning," *Sustainability*, vol. 14, no. 19, 2022.

[18] M. Rimondi, R. Mandrioli, V. Cirimele, L. K. Pittala, M. Ricco, and G. Grandi, "Design of an integrated, six-phase, interleaved, synchronous dc/dc boost converter on a fuel-cell-powered sport catamaran," *Designs*, vol. 6, no. 6, 2022.

[19] R. Bayerer, T. Herrmann, T. Licht, J. Lutz, and M. Feller, "Model for power cycling lifetime of igbt modules - various factors influencing lifetime," in *Proc. 5th Int. Conf. Integr. Power Syst.*, 2008, pp. 1–6.

[20] M. Novak, A. Sangwongwanich, and F. Blaabjerg, "Monte carlo-based reliability estimation methods for power devices in power electronics systems," *IEEE Open J. Power Electron.*, vol. 2, pp. 523–534, 2021.